Evolution of the East Greenland Current between 1150 and 1740 AD, revealed by diatom-based sea surface temperature and sea-ice concentration reconstructions

Aurélie Justwan[1,2] & Nalân Koç[1,2]

1 Norwegian Polar Institute, Polar Environmental Centre, NO-9296 Tromsø, Norway
2 Department of Geology, University of Tromsø, NO-9037 Tromsø, Norway

Keywords
Diatoms; East Greenland Current; Late Holocene; MD99-2322; sea ice; sea surface temperature.

Correspondence
Aurélie Justwan, Norwegian Polar Institute, Polar Environmental Centre, NO-9296 Tromsø, Norway. E-mail: aurelie@justwan.net

doi:10.1111/j.1751-8369.2008.00088.x

Abstract

Sediment core MD99-2322 from the East Greenland shelf has been studied to assess the variability of the East Greenland Current between 1150 and 1740 AD. Only the top 100 cm of the high-resolution core—with a 4-year resolution through the upper 20 cm, and a 10-year resolution through the remaining section—was studied. Diatoms were utilized to reconstruct both the August sea-surface temperature (SST) and the May sea-ice concentration, using the weighted averages–partial least squares and maximum likelihood transfer function methods, respectively. The record can be divided into three periods: two periods of relatively stable August SSTs and May sea-ice concentrations, separated by a period of higher August SSTs and decreasing May sea-ice concentrations between 1500 and 1670 AD, and between 1450 and 1610 AD, respectively. Both trends are statistically significant, based on the SiZer (significant zero crossing of the derivatives) analysis of the records. These changes are explained by a decrease in the strength of the East Greenland Current between 1450 and 1670 AD, which was responsible for bringing cold polar water and sea ice to the core site. Simultaneous changes observed in both these parameters points to a strong coupling between them. Because of the high resolution of the record, the natural variability of the system over the period of almost 700 years can be assessed. This variability is about 1°C (±0.9°C) for August SSTs and 12% (±7.4%) for May sea-ice concentrations.

In recent years, there has been increasing concern about the evolution of the ice caps and the extent of ice in polar regions, including sea ice. This concern was prompted by reports describing the accelerated decrease of sea-ice extent, the increasing rate in the calving of glaciers and the melting of the polar ice caps (e.g., Watson 2001; Rothrock et al. 2003; Johannessen et al. 2004; Weaver & Hillaire 2004; Stroeve et al. 2005; Divine & Dick 2006; Kohler et al. 2007).

Satellite data show the expansion of the melt regions in the large land ice masses and glaciers of the Northern Hemisphere (Comiso & Parkinson 2004), which are contributing to a global rise in sea level. An important question and concern about these observed changes is whether they are "normal", meaning part of a cycle of "natural" climate variability, or whether they are caused human activity. One of the challenges in attempting to study changes in past sea-ice extent is the lack of long time series. The instrumental records of temperature in the Arctic region only extend as far back as 100 years at most. The detailed recording of sea-ice extent based on satellite imagery, which is the only technique giving a detailed picture of the spatial and temporal patterns of seasonal and interannual variability in ice extent and concentrations, only reaches 30 years back in time. This time period is too short for resolving the multi-year variability in ice cover. Information on sea ice from historical records is available for the last couple of hundred years, but this information is often regional and discontinuous (e.g., Vinje 1999, 2001; Ogilvie et al. 2000).

The purpose of the present study is to assess the multi-year variability of the East Greenland Current (EGC), which is the main conduit of sea ice and freshwater from

the Arctic Ocean to the North Atlantic, using August sea-surface temperature (SST) and May sea-ice concentration reconstructions with diatom-based transfer functions. The study will provide a time series of these parameters that is longer than has heretofore been available, offering a longer time perspective on the current changes. With these objectives, we analysed a sediment core from a high sediment accumulation setting off the coast of East Greenland. The studied section covers the time interval from 1150 to 1740 AD, as the top of the core is dated to 200 cal years B.P. The core was analysed with a resolution of around 4 years from 1720 to 1600 AD, and with a resolution of around 10 years for the rest of the record (1600–1150 AD). The August SST was reconstructed using diatoms and a transfer function based on the weighted averages–partial least squares (WA–PLS) method. The May sea-ice concentration was reconstructed from diatoms using the maximum likelihood (ML) method. To evaluate the significance of reconstructed changes, the generated time series were further analysed by SiZER (significant zero crossing of the derivatives).

Oceanographic setting

The sediment core MD99-2322 is located on the East Greenland shelf in the Kangerlussuaq Trough (67°08.18N, 30°49.67W; Fig. 1). The site is mainly influenced by the EGC, which transports cold and low-salinity water, and underlying Atlantic intermediate water, southwards along the East Greenland margin (Aagaard & Coachman 1968a, 1968b; Johannessen 1986). The path of the EGC also corresponds to the path followed by the distribution of pack ice and fresh water releases from the Arctic Ocean.

Surface ocean currents are driven by atmospheric circulation, which in turn is influenced by the distribution of sea ice and water masses (Rodwell et al. 1999; Deser et al. 2000). The atmosphere directly influences sea-ice anomalies through wind-driven ice drift, and by advection of warm air towards the ice edge (Deser et al. 2000). Under the influence of northern winds, the polar water and sea ice advance southwards along the East Greenland margin. This lowers the surface salinity of the EGC to 34.4, such that it is effectively stratified, thereby allowing sea ice to form in situ. Martin & Wadhams (1999) have shown that sea-ice drift velocities exhibit seasonal variations, with high velocities of up to 0.1 m s^{-1} on average for the winter months, and 0.05 m s^{-1} for the summer months.

During the last 50 years, decadal-scale oceanic variability has been observed in the high-latitude North Atlantic. Dramatic changes in freshwater and sea-ice distribution coincide with the "Great Salinity Anomalies" (GSAs; Sigtryggsson 1972; Dickson et al. 1988). The first observed GSA originated from the large change in sea-ice

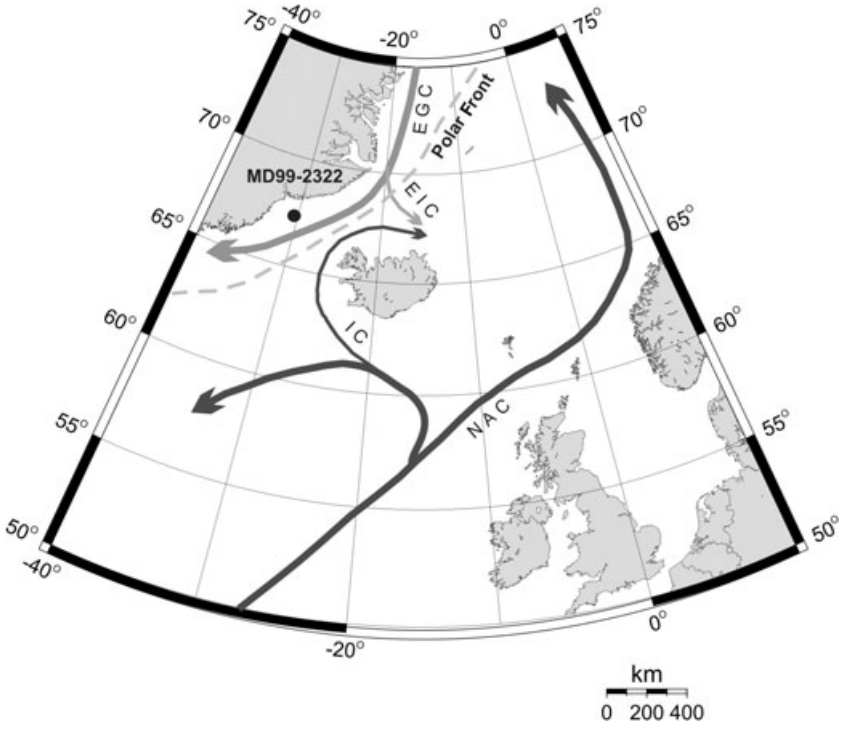

Fig. 1 Map showing the core location in relation to the main surface currents in the area. Abbreviations: EGC, East Greenland Current; EIC, East Icelandic Current; IC, Irminger Current; NAC, North Atlantic Current.

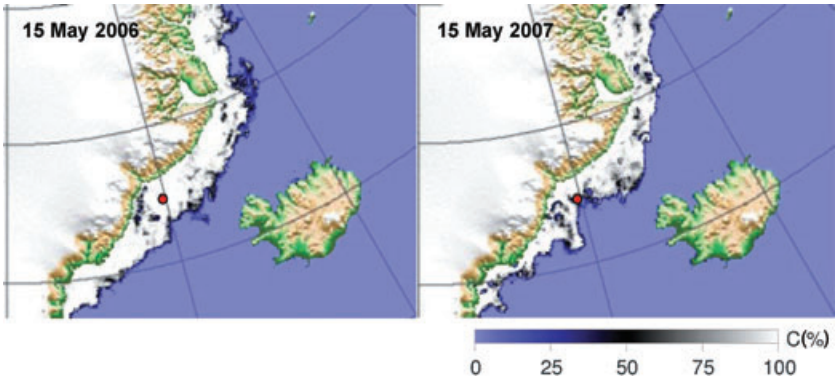

Fig. 2 Advanced Microwave Scanning Radiometer for EOS (AMSR-E) images of sea-ice concentration for 15 May 2006 and 15 May 2007 (Spreen & Kaleschke 2008). The core location is indicated by the red dot.

flux through Fram Strait in 1968 (Serreze et al. 1992). Later GSAs occurred in the 1980s and the early 1990s in the subpolar gyre (Belkin et al. 1998). GSAs are a consequence of the fact that polar water and sea ice advance beyond their normal limits in the EGC, to bring cold, low-salinity polar waters into the East Icelandic Current (EIC) and the subpolar gyre. The years with the most severe sea ice along the East Greenland and Iceland coasts have a similar pattern, with the sea ice moving into the EIC and advancing around the eastern coast of Iceland in the spring, and pushing the oceanic polar front southwards (Sigtryggsson 1972).

Divine & Dick (2006) show that the maximum of the sea-ice edge occurs during the months of April and May in the Nordic seas, and that both the maximum and the minimum positions of the ice edge have been retreating towards the East Greenland coast since 1870. This retreat can also be observed at the core site. Their analyses also provide evidence for the presence of a 70-year periodicity, as well as for a pronounced two- to three-decadal variability in the Greenland Sea. Recent satellite images show that during 2006 our core site was covered with sea ice during May, whereas in 2007 it was at the ice edge, reflecting the year-to-year variability of the system superimposed on this general trend of decrease (Fig. 2).

Modern summer SSTs reach a maximum at the core site between 5 and 6°C, and the salinity is around 34.4 (Hopkins 1991; Conkright et al. 2002). This is because the polar water layer is thin and quite strongly stratified, and therefore warms up during summer.

Material and methods

Material

The East Greenland shelf is incised by deep, cross-shelf troughs, which are below the depth of iceberg scouring, and act as efficient sediment traps (Andrews et al. 1994). Core MD99-2322 was collected on the eastern Greenland shelf (67°08.18N, 30°49.67W) (Fig. 1) from the deepest part of the Kangerlussuaq Trough, at a water depth of 714 m during the IMAGES cruise, Leg 4, in 1999, aboard the French vessel RV *Marion Dufresne*. The 26.17-m long Calypso core consists of homogeneous dark-grey silty clays of Holocene age (Jennings et al. 2005; Stoner et al. 2007). The X-ray photographs of the core show occasional mm- to cm-thick sandy silt lenses and dispersed grains of less than 1 mm in diameter, which are interpreted as ice-rafted debris. There is no indication of discernable bioturbation structures, nor is there evidence for deformation or stretching in the section studied. Any significant bioturbation would have caused a smoothing effect in the climate time series generated. However, we do not observe this, even in the interval sampled at a resolution of 0.5 cm. The magnetic susceptibility record shows a smooth trend, indicating that there are no dramatic changes in sedimentation. In this study we focus on the latest part of the Holocene, covering the last 1000 years. For this purpose, only the upper 1 m of the core was sampled. The top 20 cm of the core was sampled every 0.5 cm to achieve a resolution of 3–4 years. The rest of the section was analysed every 1 or 2 cm to achieve a resolution of about 10 years.

Sample preparation

Samples were cleaned for diatom analyses using the method described by Koç et al. (1993), which consists of chemically cleaning the samples to remove calcium carbonate and organic matter, using hydrochloric acid and hydrogen peroxide, followed by a differential settling method to remove clay particles. Quantitative slides were prepared following the method described by Koç & Schrader (1990). Each slide was observed using a Leitz Orthoplan microscope with a 100/1.32 magnification. A minimum of 300 *Chaetoceros* spp.-free diatom valves were counted, following the procedure described by Schrader & Gersonde (1978).

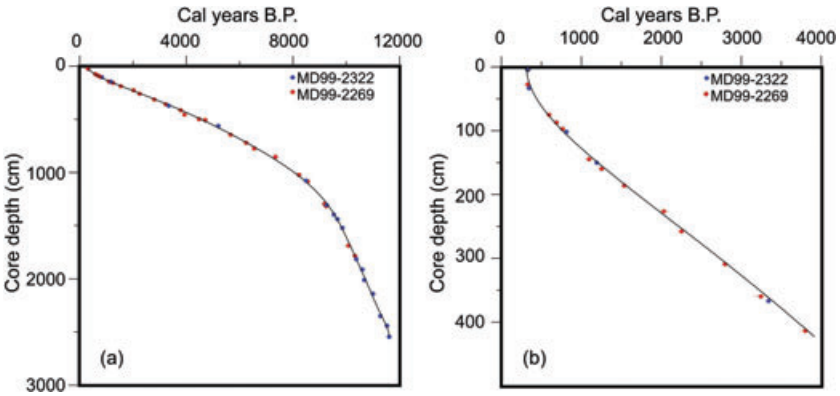

Fig. 3 (a) Age model for core MD99-2322, based on a ninth-order polynomial fitting between calibrated ^{14}C dates from MD-99-2322 and from MD99-2269, which have been depth-correlated using palaeomagnetic secular variation (PSV) (from Stoner et al. 2007). (b) Age versus depth relationship for the uppermost 400 cm of core MD99-2322, highlighting the fit of the polynomial function.

Core chronology

A model for core MD99-2322 with exceptionally high age resolution has been developed by Stoner et al. (2007), based on the ninth-order polynomial fitting of 19 accelerator mass spectrometry (AMS) ^{14}C dates from core MD99-2322, 27 AMS ^{14}C dates from core MD99-2269 on the North-West Iceland shelf, tephrochronology and palaeomagnetic secular variation (PSV) records of both cores, which we have also used in this study (Fig. 3). Even though there were originally only three AMS ^{14}C dates available for the section studied in core MD99-2322, using the approach of Stoner et al. (2007), the age control of the studied section is highly improved with the transfer of five additional AMS ^{14}C dates from core MD99-2269 to the combined age–depth model (Table 1), together with the PSV correlations. The calibrated ages for core MD99-2322 are presented in Table 1, along with their ranges. Stoner et al. (2007) calibrated the ^{14}C dates to cal years B.P. (1950) using CALIB 5.0 (Stuiver & Reimer 1993), and the updated marine calibration data sets (Hughen et al. 2004) with a standard marine reservoir correction of 400 years. The dates cited in this study are all presented in calibrated age AD. The core-top date for core MD99-2322 is 675 ± 30 ^{14}C years B.P., with a 1σ calibration to 277, 322, and 360 cal years B.P., indicating the lack of sediments from the last 250 years. It is, however, not uncommon for giant Calypso coring systems to blow off the top soft sediments (see, for example, Andersen et al. 2004: table 2, for core MD95-2011). We do not, therefore, think the lack of recent sediments reflect a halt in sedimentation in the area. On the contrary, the decreasing sea-ice cover since 1870, as shown by Divine & Dick (2006), should indicate an increased sedimentation rate.

Reconstruction of the August SSTs and May sea-ice concentrations using transfer functions

August SSTs and May sea-ice concentrations are reconstructed using transfer functions based on diatom species counted downcore. Diatoms are single-celled phytoplankton; as such, they are dependent on light to survive, and therefore live in the uppermost part of the oceans. Diatoms have over the years proven to be an excellent tool for palaeoclimatic reconstructions in high-latitude oceans, especially in the Nordic seas (Koç & Schrader 1990; Koç-Karpuz & Jansen 1992; Koç et al. 1993) because of their high productivity and diversity. A modern training set consisting of 139 surface samples with 52 diatom species (Andersen et al. 2004) has been used to develop the August SST transfer function (Justwan et al. 2008). In this study, the WA–PLS method is used for the August SST reconstruction. The reasons behind this choice are explained in detail in Justwan et al. (2008). The sea-ice concentration transfer function is based on a modern training set consisting of 99 surface sediment samples with 52 diatom species (Justwan & Koç 2007). The ML method is used for reconstructing the May sea-ice concentrations. The reasons behind this choice are further explained in Justwan & Koç (2007). The uncertainties of the August SST and May sea-ice concentration reconstructions (95% confidence interval) are ±0.9°C and ±7.4%, respectively. Both transfer functions have proven to be very useful tools for palaeoclimatic reconstruction, and have been applied to a number of cores in the North Atlantic (Justwan & Koç 2007; Berner et al. 2008; Justwan et al. 2008).

SIZER analysis of the time series

SIZER (Chardhuri & Marron 1999) is applied to the generated time series to explore significant features in the August SST and May sea-ice time series, which might have been otherwise overlooked. SIZER is a statistical method for finding structure in time series, and helps in defining periods with significant common climatic development. The method is based on "scale space" ideas (Chardhuri & Marron 1999). Scale space is a family of

Table 1 Accelerator mass spectometer radiocarbon measurements and calibrated (calendar) ages for the age model of core MD99-2322, including dates from core MD99-2269, which have been depth-correlated using palaeomagnetic secular variation (PSV) (from Stoner et al. 2007) for the interval studied.

Core	MD99-2322 depth (cm)	Material dated	Calibrated calender ages		
			Min. 1σ	Med. prob.	Max. 1σ
MD99-2269	28	*Arca glacialis*	281	328	364
MD99-2269	75	*Macoma* sp.	556	590	623
MD99-2269	87	cf. *Macoma balthica*	644	679	711
MD99-2269	98	*Bathyarca glacialis*	718	762	795
MD99-2269	145	mixed forams	1 036	1 091	1 161
MD99-2269	160	*Macoma* sp.	1 210	1 250	1 293
MD99-2269	187	cf. *Yoldia glacialis*	1 489	1 536	1 593
MD99-2269	227	cf. *Macoma balthica*	1 966	2 028	2 098
MD99-2269	258	*Yoldia cf. myalis*	2 189	2 247	2 315
MD99-2269	310	*Yoldia* sp.	2 741	2 787	2 824
MD99-2269	360	mixed forams	3 142	3 237	3 345
MD99-2269	415	*Arca glacialis*	3 730	3 793	3 845
MD99-2269	456	*Yoldia* sp.	3 866	3 939	3 992
MD99-2269	497	cf. *Nucula*	4 407	4 474	4 527
MD99-2269	507	unid. gastropod	4 638	4 703	4 793
MD99-2269	644	*Yoldia cf. lenticula*	5 592	5 657	5 704
MD99-2269	719	*Yoldia sp.*	6 192	6 245	6 289
MD99-2269	853	mixed forams	7 274	7 351	7 419
MD99-2269	1017	*Yoldia glacialis*	8 159	8 222	8 298
MD99-2269	1079	cf. *Macoma balthica*	8 458	8 545	8 608
MD99-2269	1294	*N. labradorica*	9 106	9 219	9 330
MD99-2269	1308	unid. molluscs	9 162	9 251	9 325
MD99-2269	1685	unid. molluscs	9 966	10 085	10 193
MD99-2269	1780	mixed forams	10 227	10 336	10 425
MD-99-2322	2.5	*Astarte* sp.	277	322	360
MD-99-2322	34	*Colus turgidulus*	290	344	385
MD-99-2322	101.5	mixed forams	761	812	875
MD-99-2322	150	bivalve	1 146	1 191	1 250
MD-99-2322	368	bivalve	3 280	3 332	3 381
MD-99-2322	564	scaphopod	5 125	5 213	5 299
MD-99-2322	771	shell fragments	6 467	6 545	6 626
MD-99-2322	1073	*Nuculuna buccata*	8 170	8 522	8 883
MD-99-2322	1298	*Nuculuna pernula*	9 189	9 272	9 385
MD-99-2322	1393	*Nuculuna pernula*	9 466	9 535	9 595
MD-99-2322	1432	*Bathyarca glacialis*	9 552	9 679	9 755
MD-99-2322	1516	*Nuculuna buccata*	9 716	9 859	9 999
MD-99-2322	1807	*Nuculuna buccata*	10 273	10 369	10 466
MD-99-2322	1908	*Nuculuna buccata*	10 519	10 616	10 692
MD-99-2322	2006	*Nuculuna buccata*	10 567	10 675	10 751
MD-99-2322	2140	*Nuculuna buccata*	10 921	11 017	11 143
MD-99-2322	2342	*Nuculuna buccata*	11 180	11 296	11 375
MD-99-2322	2436	*Nuculuna pernula*	11 345	11 547	11 706
MD-99-2322	2542	benthic forams	11 365	11 621	11 851

Gaussian smoothing functions indexed by the bandwidth, shown as blue curves in the family plot, and is based on data shown as green dots (see Fig. 5). At each data point, a local linear kernel estimator is used to produce smooths of the estimated sea ice or temperature. SiZer studies the significance of zero crossings of the derivative of the smooths in scale space, as shown on the SiZer plot. It represents regions with respect to both location and scale with colours. Red is used where the smooth is significantly decreasing, blue is used for significantly increasing and the intermediate colour purple is used for no significant slope. The thick red curve in the family plot corresponds to the smooth with the bandwidth corresponding to the solid black line in the SiZer plot (see Fig. 5; Kim & Marron 2006). The zero crossings are used directly to define periods in the record.

Performing this statistical analysis allows an interpretation of climatic change to be made with higher confidence, as visual inspection of climatic reconstruction often results in an underestimation or an overestimation of the statistical significance of variations.

Results

Diatom flux variation

Downcore diatom abundances (number of valves per gram of dry sediment) are converted to diatom flux in order to infer past diatom productivity. The diatom flux values can be used as a proxy for productivity, even though the flux is influenced by both productivity and dissolution/preservation of diatoms in the water column. We assume here that surface productivity is the main driver of changes in diatom flux.

The variation of the diatom flux in core MD99-2322 between 1150 and 1740 AD is characterized by two periods of higher flux, separated by a period of lower flux, between 1325 and 1550 AD (Fig. 4). The period between 1150 and 1325 AD is characterized not only by high flux values, but also by high variability. At the end of this period, the flux decreases rather abruptly over a 50-year interval. The other high flux period, between 1550 and 1740 AD, is characterized by slightly lower flux values, and also has less variability in amplitude. The increase in flux spans a period of 75 years. The low flux period is characterized by extremely low variability, indicating stable low surface productivity throughout this period. The productivity between 1150 and 1740 AD can be characterized by two periods of high productivity, separated by a period of low surface productivity between 1325 and 1550 AD. The first period of high productivity (1150–1325 AD) shows high variability. The second period of high productivity (1550–1740 AD) appears to be more stable. The period of higher productivity can be attributed to a stronger inflow of polar waters, which are rich in nutrients, transported by the EGC (Hopkins 1991).

Fig. 4 Diatom flux of core, in valves per gram per year, at site MD99-2322.

August SST reconstruction

The August SST, reconstructed using the WA–PLS transfer function (Justwan et al. 2008.), records August SSTs between 6.5 and 8.5°C, and variability of up to 1.5°C, in the time period 1140–1740 AD (Fig. 5). The August SST record was further analysed using the SIZER software (Chardhuri & Marron 1999) to give a higher confidence level for the observed changes. The analysis shows that there is a slight warming trend throughout the interval studied. In more detail, the analysis shows that the record can be divided into three periods: two periods of lower August SSTs, of around 7°C between 1150 and 1500 AD, and between 1670 and 1740 AD, separated by a period of warmer August SSTs, of around 7.5°C (Fig. 5). The SST difference between the colder and warmer periods is close to the standard error of the transfer function; however, the increase and decrease in August SSTs bracketing the warmer interval are statistically significant, as determined by the SIZER analysis. As such, we conclude that this period is different from the two other periods with lower August SSTs.

Higher frequency changes are superimposed on these three periods. They seem to be the result of true changes, and are not merely the result of noise, as they are most often defined by several sample points. The higher frequency changes vary from 0.5 to 1.5°C: changes that in some cases are close to the ± 0.9°C standard error of the reconstruction. However, as these changes are also accompanied with changes in the composition of diatoms, we are confident that the changes are real, but the uncertainties associated with our reconstruction techniques make it difficult to fully quantify the magnitude of these changes at the present time.

May sea-ice concentration reconstruction

The sea-ice time series was also analysed using SIZER so as to interpret changes in May sea-ice concentration with a higher confidence, and to avoid any under- or overinterpretation of the recorded variability. The May sea-ice concentration record between 1150 and 1740 AD is characterized by a general decreasing trend, from values around 22% to values of around 14% (Fig. 6). Using the results of the SIZER analysis, the record can be subdivided into three periods: two periods of fairly constant May sea-ice concentration, between 1150 and 1450 AD, with May sea-ice concentrations of around 19%, on average, and between 1610 and 1740 AD, with May sea-ice concentrations of around 16%, on average. These two periods are separated by a statistically significant decrease in May sea-ice concentration of 12% over a 160-year period (determined by SIZER analysis). This decrease is significantly higher than the ±7.4% standard error of the reconstruction method. Another interesting feature of the record is its high variability, which is often within the standard error of the method. This high variability could result from noise in the record, or might reflect a true, higher incidence of sea-ice variability. The fact that more than one data point defines a high-frequency variation corroborates that these variations are real, and not merely the result of noise.

Discussion

Possible mechanisms

As described above, the August SST record is divided into three periods, which reflects changes in the heat content of the surface currents in the EGC. A cooling in the record can be explained by a stronger EGC, transporting more polar water along the east coast of Greenland. Therefore, the variations observed in the August SST record can be explained by changes in the flux of polar water transported by the EGC: periods of "warmer" SST reflect periods of decreased transport, and periods of "colder" August SST reflect a stronger transport of polar water by the EGC.

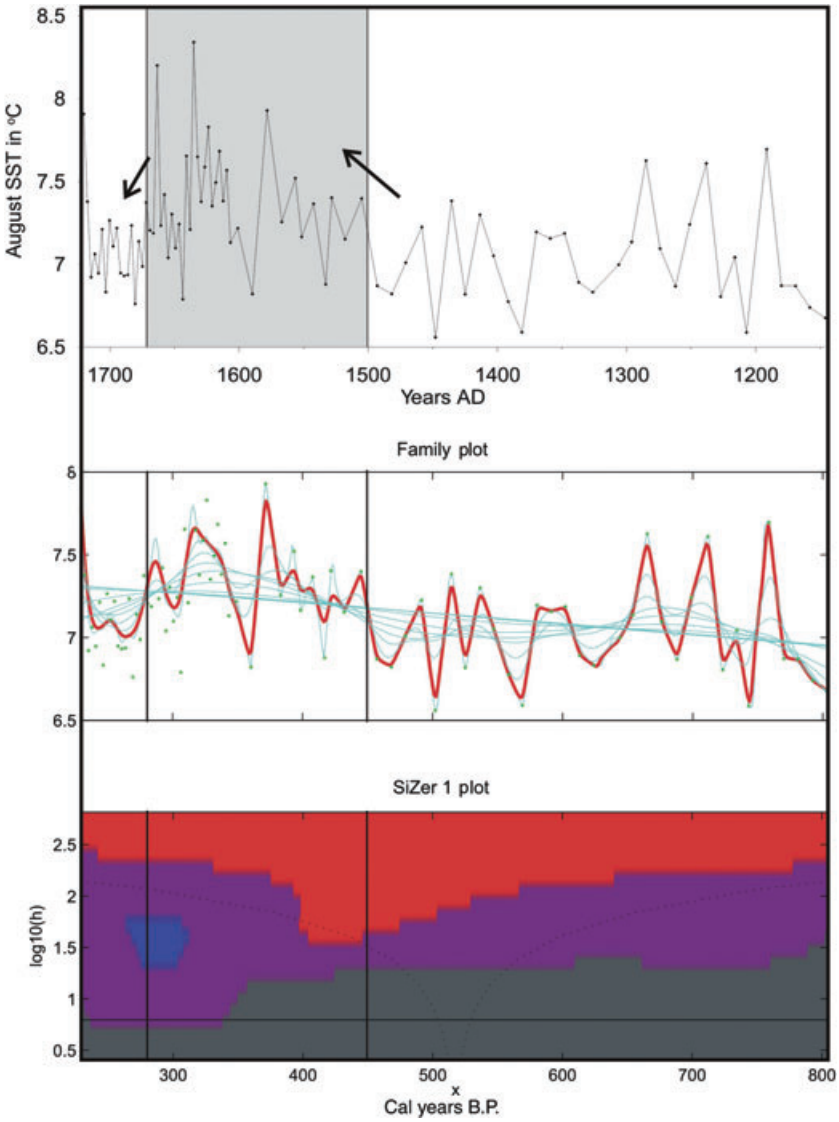

Fig. 5 August sea-surface temperature (SST) reconstruction displayed alongside the SiZer analysis for core MD99-2322. The family plot shows smoothing at different scales. The green dots represent the raw data, and the red line illustrates the general smoothing of the record. The SiZer map is given as a function of location of scale. A significant decrease is flagged as blue, whereas a significant increase is flagged as red. The colour purple is used at locations where the derivative is not found to be significantly different from zero. The colour grey in the lowermost plot is used to indicate periods in which too few data are available to perform an analysis. Typically, the colour grey occurs on very small scales for SiZer plots. The periods of warmer August SSTs are highlighted in grey shading. The record is presented with both AD and cal years B.P. scales.

The general trend in the sea-ice concentration between 1150 and 1740 AD is a weak decrease, with two periods of stable average May sea-ice concentration, separated by a period of 12% decrease over a 160-year interval (Fig. 6). The sea ice observed at the site has two origins: it is either formed in situ or is transported from northern Greenland through the Fram Strait. Walsh & Chapman (1990) described a mechanism that could account for an increase in sea-ice concentration at the site studied. In a situation with strong anomalous westerly winds in the Arctic, ice would be driven from the waters offshore of Canada and northern Greenland into the outflow region near the Fram Strait. This would result in an enhanced flux of relatively fresh water and sea ice into the Fram Strait region. The increased export of low-salinity water out of the Arctic into the Greenland Sea strengthens the halocline, which in turn is favourable to the formation of sea ice in situ. This mechanism can in fact account for an increase in both in situ and transported sea-ice from the EGC. Furthermore, this mechanism has the greatest influence in the summer season, and as such is most likely to be recorded by the diatoms, because they represent a spring/summer signal.

The positive mode of the Arctic Oscillation enhances ice advection away from the coast of the East Siberian and Laptev seas, and increases ice export out of Fram Strait (Rigor et al. 2002). The Transpolar Drift transports sea ice from the East Arctic to the West Arctic Ocean over the Fram Basin, across the North Pole, resulting in ice export out of the Fram Strait to lower latitudes, where the ice melts on meeting warm Atlantic waters. The positive mode of the North Atlantic Oscillation index is also

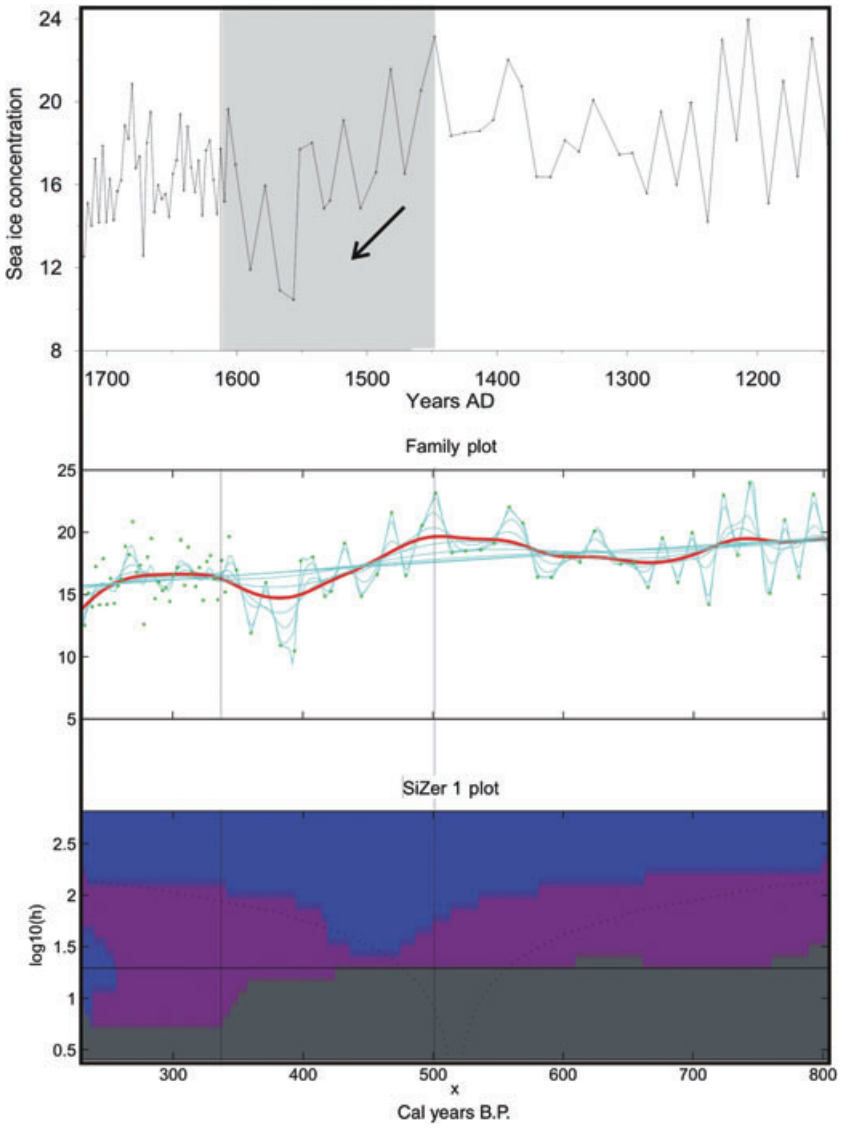

Fig. 6 May sea-ice concentration reconstruction for core MD99-2322 given as a % displayed alongside the SiZer analysis. The periods of decreasing May sea-ice concentration are highlighted in grey shading. The record is presented with both AD and cal years B.P. scales.

correlated with the areal flux of ice export through Fram Strait (Kwok & Rothrock 1999). The two periods (1150–1450 and 1610–1740 AD) with relatively higher sea ice concentrations documented in our record can therefore be related to climatic conditions, which are similar to positive modes of the Arctic Oscillation and the North Atlantic Oscillation.

Sea-ice variability

Our record of August SSTs shows a general warming trend, and the May sea-ice concentration shows a general decrease throughout the period studied between 1150 and 1740 AD (Fig. 7). Persistent ice retreat since the second half of the 19th century has already been shown by Divine & Dick (2006), indicating a continuation of this negative trend for sea ice from 1150 AD up to the present. However, they also showed that the retreat of ice is not uniform, but includes periods of advances (in the 1860s, 1880s, 1910s, 1940s, 1960s and 1980s) within the general trend.

Reconstruction of the ice-volume transport through Fram Strait over the last 50 years indicates decadal variability in relation to sea-level pressure changes over the Arctic Ocean (Vinje 2001). Using historical records, Divine & Dick (2006) reconstructed the sea-ice edge position for East Greenland between 1750 and 2002 AD. They subsequently applied wavelet analysis to the sea-ice edge anomalies time series. They observed a 24–30-year mode of ice-edge variability between April and August. This cyclicity has also been observed by several authors, both in instrumental (Delworth & Mann 2000) and in proxy

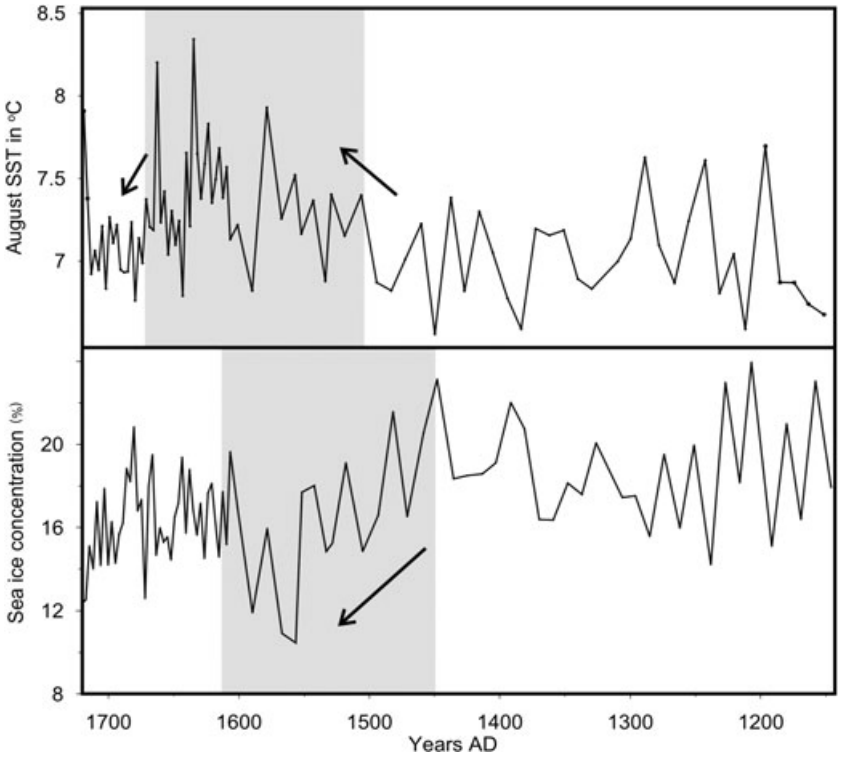

Fig. 7 Comparison between August sea-surface temperature (SST) and May sea-ice concentration reconstructions. The periods of decrease in May sea-ice concentration and warmer August SSTs are highlighted.

records (Mann et al. 1995; Gray et al. 2004; Isaksson et al. 2005), who have attributed this variability to changes in the thermohaline circulation. A 30–40-year periodicity also appears to be present in our record. However, this periodicity cannot be resolved here with high confidence, as the resolution of the record is not optimal between 1150 and 1600 AD, and because the section with higher resolution is too short to observe such cyclicity. An increase in both the interval studied and the resolution would be needed to resolve any cyclicity in the record with more certitude.

Coupling between sea ice, SST and currents

The two reconstructed records are nearly mirror images of each other, showing that an increase in sea-ice concentration is accompanied by a cooling of the surface waters, and vice versa (Fig. 7). As these reconstructions are based on two different transfer functions, this cannot be a methodological artefact. We conclude, therefore, that these two parameters have been closely coupled on the East Greenland shelf throughout the interval studied. This coupling can even be observed in the high-resolution interval (1600–1740 AD), where the changes are less pronounced.

Reconstructed summer SSTs off northern Iceland show a generally colder period between 1300 and 1600 AD (Jiang et al. 2005). This study is also based on diatom assemblages using the same transfer function method (WA–PLS), but with a different set of surface sediment samples and environmental variables. Cooling of surface waters is also observed over the East Greenland shelf between 1300 and 1500 AD (Fig. 5). A similar decrease in August SSTs between 1300 and 1600 AD is observed in cores from both the Labrador Sea and north of Iceland (Andersen 2003). However, these cores, which have higher resolution in this interval, also show a warming between 1400 and 1450 AD. These different reconstructions reinforce the hypothesis that a decrease in the reconstructed August SST at the MD99-2322 core site resulted from an increase in the strength of the EGC, which also increases the strength of the EIC. The strong influence of the polar waters at the site studied is also observed in the study of foraminifera assemblages in MD99-2322 (Jennings et al. 2005). In the present record, there is no period that can clearly be attributed to the "Little Ice Age" or the "Medieval Warm Period". However, the record only spans from 1150 to 1740 AD. At a site off south-west Greenland, where the diatom assemblage has been studied, the Little Ice Age is observed to have occurred between 1580 and 1850 AD, and the Medieval Warm Period is observed to have occurred between 960 and 1140 AD (Jensen et al. 2004). The fact that a cooling associated with the Little Ice Age is not obvious in the

records can be related to the fact that the record does not span the complete Little Ice Age period.

Superimposed on the large-scale variation of both August SSTs and May sea-ice concentrations is a higher frequency variability. This high-frequency variability is interesting, because it represents the short-term natural variability of the system, as the record predates the industrial revolution. The decadal variation in the record does not seem to exceed 1°C in August SSTs and 12% variability in May sea-ice concentration. This indicates a natural variability of the system, without the long-term trend, of around 1°C and 12% over a decade. Even though this variability is close to the standard error of the transfer functions, ±0.9°C and ±7.4 %, respectively, for August SSTs and May sea ice-concentrations, based on observations of assemblage changes, we argue that the variability is real.

Conclusions

A persistant, but variable, retreat of the sea ice is recorded off south-east Greenland since 1150 AD. The MD99-2322 record indicates a rather dynamic EGC between 1150 and 1740 AD. However, the magnitudes of the reconstructed changes are not large: with variabilities of 1°C in August SST and 12% in May sea-ice concentration. Simultaneous changes observed in both these parameters point to a strong coupling between them. Two periods (1150–1450 AD and 1610–1740 AD) with relatively higher sea-ice concentrations are documented in the EGC region. These periods can be associated with climatic conditions that are similar to positive modes of the Arctic Oscillation and the North Atlantic Oscillation. Similar palaeoceanographic changes observed both under the EGC and the EIC indicate a close coupling between these two current systems.

High-resolution quantitative time series reconstructions of climate parameters are essential, as they enable the assessment of the natural variability of the system, and as such can be used to better understand the climate system as well as improve climate models and, in turn, their forecasts.

Acknowledgements

The research for this paper was supported by the Norwegian Polar Institute, the Research Council of Norway through the MACESIZ project and the European Commission PACLIVA project. The authors are indebted to Anne E. Jennings for providing the core samples for this study. Fred Gotliebsen is thanked for assistance with the SIZER analysis. H. Justwan is thanked for his comments on previous versions of the manuscript.

References

Aagaard K. & Coachman L.K. 1968a. The East Greenland Current north of Denmark Strait: part I. *Arctic 21*, 181–200.

Aagaard K. & Coachman L.K. 1968b. The East Greenland Current north of Denmark Strait: part II. *Arctic 21*, 267–290.

Andersen C. 2003. *Surface ocean climate development and heat flux variability in the Nordic seas and the subpolar North Atlantic during the Holocene*. DSc thesis, University of Bergen.

Andersen C., Koç N., Jennings A.E. & Andrews J.T., 2004. Nonuniform response of the major surface currents in the Nordic seas to insolation forcing: implications for the Holocene climate variability. *Paleoceanography 19*, PA2003, doi: 10.1029/2002PA000873.

Andrews J.T., Milliman J.D., Jennings A.E., Rynes N. & Dwyer J., 1994. Sediment thickness and Holocene glacial marine sedimentation rates in three East Greenland fjords (ca. 68°N). *The Journal of Geology 102*, 669–683.

Belkin I.M., Levitus S., Antonov J.I. & Malmberg S.-A. 1998. "Great Salinity Anomalies" in the North Atlantic. *Progress in Oceanography 41*, 1–68.

Berner K. S., Koç N., Divine D., Godtliebsen F. & Moros M. 2008. Decadal-scale Holocene sea surface temperature record from the sub-polar North Atlantic: relation between ice-rafting episodes, regional SSTs and solar forcing. *Paleoceanography*, PA2210, doi: 10.1029/2006PA001339.

Chardhuri P. & Marron J.S. 1999. SiZer for exploration of structures in curves. *Journal of the American Statistical Association 94*, 807–823.

Comiso J.C. & Parkinson C.L. 2004. Satellite-observed changes in the Arctic. *Physics Today 8*, 38–44.

Conkright M.E., Locarnini R.A., Garcia H.E., O'Brian T.D., Boyer T.P., Stephens C. & Antonov J.I., 2002. *World Ocean Atlas 2001*. Silver Spring, MD: National Oceanographic Data Center.

Delworth T. & Mann M. 2000. Observed and simulated multi-decadal variability in the Northern Hemisphere. *Climate Dynamics 16*, 661–676.

Deser C., Walsh J.E. & Timlin M.S. 2000. Arctic sea ice variability in the context of recent atmospheric circulation trends. *Journal of Climate 13*, 617–633.

Dickson R.R., Meincke J., Malmberg S.-A. & Lee A.J. 1988. The "Great Salinity Anomaly" in the northern North Atlantic, 1968–1982. *Progress in Oceanography 20*, 103–151.

Divine D. & Dick C. 2006. Historical variability of sea ice edge position in the Nordic seas. *Journal of Geophysical Research—Oceans 111*, C01001, doi: 10.1029/2004JC002851.

Gray S., Graumlich L., Betancourt J. & Pederson G. 2004. A tree-ring based reconstruction of the Atlantic Multidecadal Oscillation since 1567 AD. *Geophysical Research Letters 31*, L12205, doi: 10.1029/2004GL019932.

Hopkins T.S. 1991. The GIN-Sea—a synthesis of its physical oceanography and literature review 1972–1985. *Earth-Science Reviews 30*, 175–318.

Hughen K.A., Baillie M.G.L., Bard E., Beck J.W., Bertand C.J.H., Blackwell P.G., Buck C.E., Burr G.S., Cutler K.B., Damon P.E., Edwards R.L., Fairbanks R.G., Friedrich M., Guilderson T.P., Kromer B., McCormac G., Manning S., Ramsey C.B., Reimer P.J., Reimer R.W., Remmele S., Southon J.R., Stuiver M., Talamo S., Taylor F.W., van der Plicht J. & Weyhenmeyer C.E. 2004. Marine04 marine radiocarbon age calibration, 0–26 kyr BP. *Radiocarbon 46*, 1059–1086.

Isaksson E., Divine D., Kohler J., Martma T., Pohjola V., Motoyama H. & Watanabe O. 2005. Climate oscillations as recorded in Svalbard ice core delta O^{18} records between AD 1200 and 1997 AD. *Geografiska Annaler 87A*, 203–214.

Jennings A.E., Andrews J.T., Woody K., Anderson D.M. & Stoner J.S. 2005. Holocene paleoceanography of the southeast Greenland shelf. American Geophysical Union, Fall Meeting 2005, abstract #PP44A-04.

Jensen K.G., Kuijpers A., Koç N. & Heinemeier J. 2004. Diatom evidence of hydrographic changes and ice conditions in Igaliku Fjord, south Greenland, during the past 1500 years. *The Holocene 2*, 152–164.

Jiang H., Eiriksson J., Schulz M., Knudsen K-L. & Seidenkrantz M-S. 2005. Evidence for solar forcing of sea-surface temperature on the north Icelandic shelf during the late Holocene. *Geology 33*, 73–76.

Johannessen O.M. 1986. Brief overview of the physical oceanography. In B.G. Hurdle (ed.): *The Nordic seas*. Pp. 103–128. New York: Springer.

Johannessen O.M., Bengtsson L., Miles M.W., Kuzmina S.I., Semenov V.A., Alekseev G.V., Nagurnyi A.P., Zakharov V.F., Bobylev L.P., Pettersson L.H., Hasselmann K. & Cattle H.P. 2004. Arctic climate change; observed and modelled temperature and sea-ice variability. *Tellus A: Dynamic Meteorology and Oceanography 56*, 328–341.

Justwan A. & Koç N. 2007. A diatom based transfer function for reconstructing sea ice concentration in the North Atlantic. *Marine Micropaleontology 66*, 264–278.

Justwan A., Koç N. & Jennings A.E. 2008. Evolution of the Irminger and East Icelandic current systems through the Holocene, revealed by diatom-based sea surface temperature reconstructions. *Quaternary Science Reviews 27*, 1571–1582.

Kim C.S. & Marron J.S. 2006. SiZer for jump detection. *Journal of Nonparametric Statistics 18*, 13–20.

Koç N., Jansen E. & Haflidason H., 1993. Paleoceanographic reconstructions of surface ocean conditions in the Greenland, Iceland and Norwegian seas through the last 14 ka based on diatoms. *Quaternary Science Reviews 12*, 115–140.

Koç N. & Schrader H. 1990. Surface sediment diatom distribution and Holocene paleotemperature variations in the Greenland, Iceland, and Norwegian Sea. *Paleoceanography 5*, 557–580.

Koç-Karpuz N. & Jansen E. 1992. A high resolution diatom record of the last deglaciation from the SE Norwegian Sea: Documentation of rapid climate changes. *Paleoceanography 7*, 499–520.

Kohler J., James T.D., Murray T., Nuth C., Brandt O., Barrand N.E., Aas H.F. & Luckman A., 2007. Acceleration in thinning rate on western Svalbard glaciers. *Geophysical Research Letters 34*, L18502, doi: 10.1029/2007GL030681.

Kwok R. and Rothrock D.A. 1999. Variability of Fram Strait ice flux and North Atlantic Oscillation. *Journal of Geophysical Research—Oceans 104*, 5177–5189.

Mann M., Park J. & Bradley R. 1995. Global interdecaldal and century scale climate oscillations during the past five centuries. *Nature 378*, 266–270.

Martin T. & Wadhams P. 1999. Sea ice flux in the East Greenland Current. *Deep-Sea Research II 46*, 1063–1082.

Ogilvie A.E.J., Barlow L.K. & Jennings A.E. 2000. North Atlantic climate c. AD 1000. *Weather 61*, 233–251.

Rigor I.G., Wallace J.M. & Colony R.L. 2002. Response of sea ice to the Arctic Oscillation. *Journal of Climate 15*, 2648–2668.

Rodwell M.J., Rowell D.P. & Folland C.K. 1999. Oceanic forcing of the wintertime North Atlantic Oscillation and European climate. *Nature 398*, 320–323.

Rothrock D.A., Zhang J. & Yu Y. 2003. The Arctic ice thickness anomaly of the 1990s: a consistent view from observations and models. *Journal of Geophysical Research—Oceans 108*, 3083, doi: 10.1029/2001JC001208.

Schrader H.J. & Gersonde R. 1978. Diatoms and silicoflagellates in the eight metres section of the lower Pliocene of Capo Rossello. *Utrecht Micropaleontological Bulletin 17*, 129–176.

Serreze M.C., Maslanik J.A., Barry R.G. & Demaria T.L. 1992. Winter atmospheric circulation in the Arctic Basin and possible relationships to the Great Salinity Anomaly in the northern North Atlantic. *Geophysical Research Letters 19*, 293–296.

Sigtryggsson H. 1972. An outline of the sea-ice conditions in the vincinity of Iceland. *Jökull 22*, 1–11.

Spreen G. & Kaleschke L. 2008. *AMSR-E ASI 6.25 km sea ice concentration data, V5.4*. Hamburg: Institute of Oceanography, University of Hamburg. Digital media.

Stoner J.S., Jennings A.E., Kristjansdottir G.B., Dunhill G., Andrews J.T. & Hardadottir J. 2007. A paleomagnetic approach toward refining Holocene radiocarbon based chronologies: paleoceanographic records from the north Iceland (MD99-2269) and East Greenland (MD99-2322) margins. *Paleoceanography 22*, PA1209, doi: 10.1029/2006PA001285.

Stroeve J.C., Serreze M.C., Fetterer F., Arbetter T., Meier W. & Maslanik J. 2005. Tracking the Arctic's shrinking ice cover: another extreme September minimum in 2004. *Geophysical Research Letters 32*, L04501, doi: 10.1029/2004GL021810.

Stuiver M. & Reimer P.J. 1993. Extended 14C database and revised CALIB radiocarbon calibration program. *Radiocarbon 35*, 215–230.

Vinje T. 1999. Barents Sea ice edge variation over the past 400 years. In: *Extended abstracts, Workshop on Sea-Ice Charts of the Arctic. WMO/TD no. 949*. Pp. 4–6. Seattle, WA: World Meteorological Organization.

Vinje T. 2001. Anomalies and trends of sea-ice extent and atmospheric circulation in the Nordic seas during the period 1864–1998. *Journal of Climatology 14*, 255–267.

Walsh J.E. & Chapman W. 1990. Arctic contribution to upper-ocean variability in the North Atlantic. *Journal of Climate 3*, 1462–1473.

Watson R.T. (ed.) 2001. *Climate change 2001. Synthesis report. Third assessment report of the Intergovernmental Panel on Climate Change*. Cambridge: Cambridge University Press.

Weaver A.J. & Hillaire M.C. 2004. Global warming and the next ice age. *Science 304*, 400–402.